ChemComm

COMMUNICATION

View Article Online
View Journal | View Issue

Cite this: *Chem. Commun.*, 2024, **60**, 10890

Received 30th April 2024,
Accepted 2nd September 2024

DOI: 10.1039/d4cc02073a

rsc.li/chemcomm

Mechanochemically-based three-way approach for the synthesis of K-doped Cu–Fe/ZnO–Al_2O_3 catalysts for converting CO_2 to oxygenates†

Boon Ying Tay,[a] Charmain Kan,[a] Jennet Ong,[a] Shashikant U. Dighe,[ab] Amol M. Hengne,[ab] Kuo-Wei Huang,[abc] Lili Zhang,[a] Roong Jien Wong *[a] and Davin Tan *[ab]

Three ball-milling methodologies were developed to synthesize bespoke multi-metallic K-doped Cu–Fe/ZnO–Al_2O_3 catalysts for the hydrogenation of carbon dioxide. The catalytic performance of the catalysts was benchmarked against their solution-based counterparts. The catalysts synthesized by ball milling are greener, showing smaller particles, with different selectivity towards oxygenate products.

Carbon dioxide (CO_2) produced by anthropogenic activities, is one of the greenhouse gases that is largely attributed as the main culprit that causes global warming and climate change.[1] Conversely, CO_2 is an abundant source of C1 carbon, and carbon capture and utilization (CCU) strategies play a crucial role to generate a myriad of products from captured CO_2.[2] Conversion of CO_2 emitted from burning fossil fuels back into fuels, namely oxygenates offers a CO_2-neutral pathway for green energy storage and utilization.[3] In particular, the direct hydrogenation of CO_2 to form alcohols such as methanol (MeOH), ethanol (EtOH), propanol *etc.*, has gained significant research interest in recent years as these compounds are highly valuable as solvents, fuel additives, and molecular precursors.[4] The key enabler of such reactions is the catalyst, yet catalytic conversion of CO_2 to higher alcohols (EtOH and above) still remains challenging, limited by low conversions and poor selectivity.[5]

Despite this, several families of multi-metallic heterogenous catalysts have been developed that can enable conversion of CO_2 to higher alcohols, which include Cu–Zn,[6–8] Co–Mo,[9,10] Pt–Co,[11] Ru–Fe[12] *etc*. However, the synthesis of these catalysts is not trivial and typically dependent on multi-step solution protocols, which can produce a lot of liquid waste, require long reaction durations, tedious preparation, or purification steps, and use expensive or corrosive metal precursors. If the catalyst can be rapidly synthesized using green chemistry principles[13] without compromising catalytic performance, it will be highly advantageous.

Mechanochemistry can provide a remedy to this problem by circumventing the use of bulk solvents and rapidly affording the desired compounds, whilst using significantly less energy than its solution-based counterparts.[14] Previous reports have demonstrated how mechanochemical techniques such as ball milling or grinding can be used to synthesize compounds and catalysts for various reactions.[15–21] Despite the clear advantages, mechanochemical treatment can sometimes yield unexpected results.[15,16] Although the correlation between how ball milling is employed during synthesis and a catalyst's overall performance has been previously reported,[22–26] the effect on catalysts for CO_2 hydrogenation to C_{2+} products remains an area of key interest. Furthermore, mechanosynthesis of catalysts using metal oxides as precursors has the additional benefit of avoiding NO_x production from metal nitrates during the calcination step. To this end, we endeavoured to develop and compare three different mechanochemical approaches to create a multi-metallic catalyst for the hydrogenation of CO_2 to alcohols.

The selected catalyst is a K-promoted Cu–Fe on a mixed ZnO–Al_2O_3 support (**KCFZA**) and is relatively complex. **KCFZA** comprises five different metals: three transition metals (Cu, Fe, Zn), one alkali metal (K), and one group III metal (Al), yet does not contain any expensive rare-earth or noble elements, which makes it relatively cheap to produce. Cu and Zn are used as the main components (Cu–Zn family) for CO_2 adsorption and activation, and Al is used as a catalyst support to prevent Zn sintering. Small amounts of Fe (5% stoichiometry) are added as previous reports have shown that Fe can aid in the carbon chain extension to achieve higher alcohols and hydrocarbons,[8] whilst basic alkali metals such as K are added as dopants (5%

[a] *Institute of Sustainability for Chemicals, Energy and Environment (ISCE²), Agency for Science, Technology and Research (A*STAR), 1 Pesek Road, Jurong Island, Singapore 627833, Republic of Singapore. E-mail: davin_tan@isce2.a-star.edu.sg*
[b] *Institute of Materials Research and Engineering (IMRE), Agency for Science, Technology and Research (A*STAR), 2 Fusionopolis Way, Singapore 138634, Republic of Singapore*
[c] *Division of Physical Sciences & Engineering, King Abdullah University of Science and Technology, Thuwal 23955–6900, Saudi Arabia*

† Electronic supplementary information (ESI) available. See DOI: https://doi.org/10.1039/d4cc02073a

weight) to bind to CO_2 and have been shown to enhance selectivity towards higher alcohols while simultaneously suppressing the formation of hydrocarbons.[27] The solution-based synthesis procedure (**SS1**) to produce **KCFZA** was modified from the work of Heracleous *et al.*,[7] which involved a co-precipitation step using Na_2CO_3 and an incipient wetness impregnation step for K-doping (**SS1-K**). Upon reduction in H_2, the multi-metallic catalyst was then used as a benchmark for comparison of the catalytic performance.

Subsequently, three solid-state methodologies to make **KCFZA** were explored, namely: **BM1**, a hybrid solution and mechanochemical method involving ball milling doping of the catalyst made from solution; **BM2**, pure mechanochemical synthesis by direct co-precipitation in the ball mill using metal nitrates followed by K-doping in the solid-state; **BM3**, mechanosynthesis of the catalyst using metal oxides as precursors, including K-doping. **BM3** effectively replaces the use of corrosive and strongly oxidising nitrate salts and is more atom economical as it circumvents the use of sacrificial Na_2CO_3 required in the co-precipitation step, which also produces undesirable CO_2 as a by-product during the subsequent calcination step. As shown in Fig. 1 *vide supra*, comparison of the powdered X-ray diffractograms (PXRD) of **SS1-K**, **BM1**, **BM2**, and **BM3** revealed that they all had very similar patterns with comparable crystallinity. The visibly distinguishable peaks at 2θ = 43.3°, 50.5°, and 74.1° in the diffractograms correspond to the characteristic diffraction planes of Cu (111), (200), and (220), respectively. Weakly diffracting peaks at 30.1°, 33.9°, and 36.6° correspond to the reflection planes of ZnO (100), (002), and (101), respectively. The presence of Cu and ZnO is largely due to the calcination and the H_2 reduction step. Furthermore, from PXRD analysis, the mechanochemical treatment of **BM1** did not appear to affect its crystallographic structure or lead to the formation of any new polymorphic phases. Of note, the use of metal oxide precursors to make **KCFZA** *via* **BM3** can also achieve the same crystal structure for the catalyst (see Supplementary information 15, ESI†), which is advantageous since the oxide precursors are more cost effective and more benchtop stable than their nitrate counterparts; nitrate salts contain water of crystallization so their molar mass is heavier per unit mole of the metal. For example for $Al(NO_3)_3{\cdot}9H_2O$, water constitutes approximately 44% of its molar weight, and their salts are very hygroscopic.

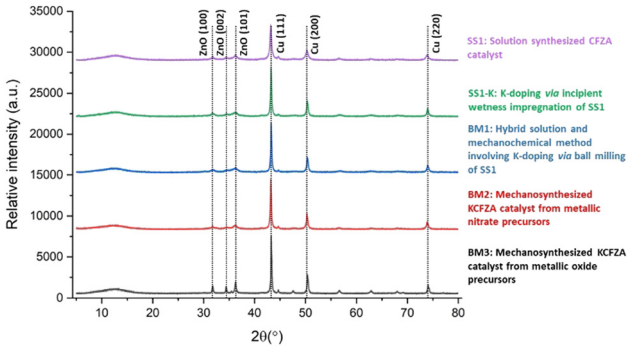

Fig. 1 X-ray diffraction patterns of the **KCZFA** catalysts prepared by mechanosynthesis, namely **BM1** (blue line), **BM2** (red line) and **BM3** (black line), and solution synthesis **SS1-K** (green line). Undoped **CFZA** catalyst by solution (**SS1**) is shown as the purple line.

Similarly, the solution and mechanochemically synthesized powdered catalysts were characterized by scanning electron microscopy coupled with energy dispersive X-ray (SEM-EDX). Initial qualitative analysis revealed that **SS1** and **SS1-K** samples largely consisted of nanocrystalline plate-like structures, with particle size ranging from 800 nm to 1000 nm (Fig. 2a) and they appeared to have aggregated. For **BM1-3**, the particles were more spherical, smaller (600–800 nm), and had a rougher surface morphology (Fig. 2b and Supplementary information 8 and 9, ESI†). This is expected and consistent with other reports that had used mechanochemistry to affect the particle size and topography of solids.[15,16,21] Furthermore, EDX analysis revealed

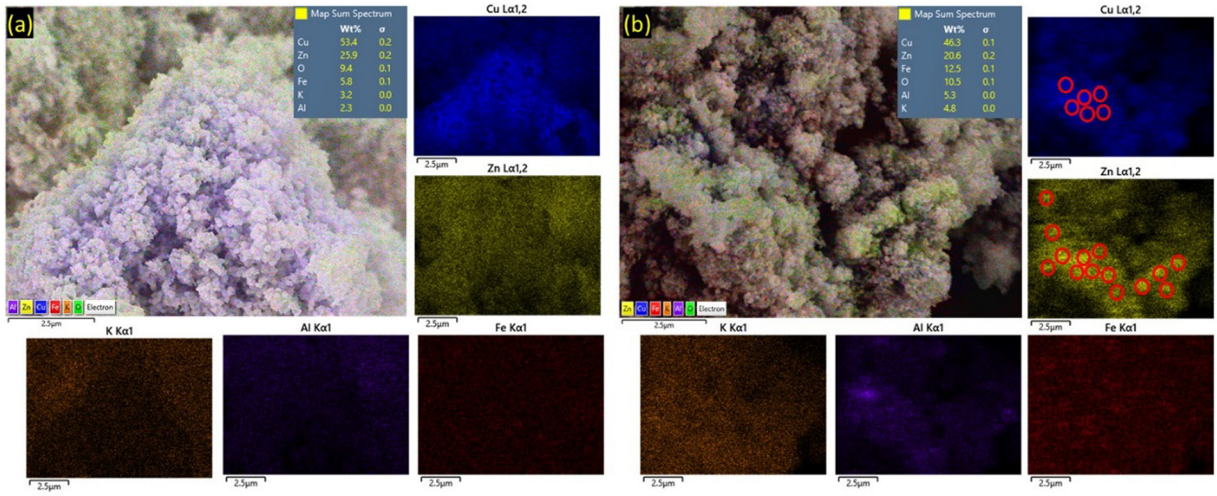

Fig. 2 SEM-EDX elemental mapping and composition of the K-doped Cu–Fe/Zn/Al (**KCFZA**) catalyst synthesised (a) by the solution method *via* **SS1-K**, using metal nitrate salt precursors and (b) by mechanochemistry *via* **BM3**, using metallic oxide precursors. Zones of aggregated metals are highlighted in the red circles.

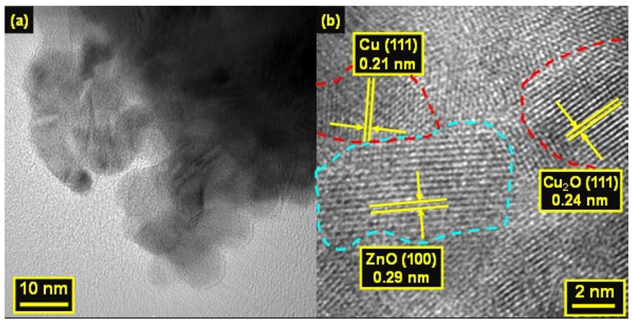

Fig. 3 (a) HRTEM images of the **BM3** catalyst, and (b) observed lattice *d*-spacings.

that the elemental composition was relatively homogenous within each sample, and they did not differ significantly from one another. This is also confirmed by PXRD Scherrer analysis (Supplementary information 16, ESI†) and ICP-OES analysis (Supplementary information 20, ESI†). Of note, in the **BM3** sample, EDX mapping appeared to show localized aggregated zones of Cu and Zn. This could be due to the use of harder metal oxide precursors that make it more difficult to achieve complete mixing during ball milling. Nonetheless, these zones constituted a very small amount of the metals as the particle sizes are very small. Overall, these results are highly promising as they demonstrate how **KCFZA** can be made without involving any solution-based reactions in the solid state *via* **BM3**.

High resolution transmission electron microscopy (HRTEM) with EDX was also employed to compare **SS1-K** (pure solution synthesis) and **BM3** (pure mechanosynthesis) samples. Indeed, the particles are rounder and smaller for **BM3**, 8–12 nm (Fig. 3), than **SS1-K**, 10–16 nm (Supplementary information 11, ESI†). The lattice *d*-spacing for the Cu (111) and (200), and Cu_2O (111) and ZnO (100) were also observed under high magnification. EDX mapping revealed a sparse but uniform elemental distribution for both samples. In **BM3**, some particles appeared to contain more Zn than others (Supplementary information 13, ESI†), which could have created the aggregated zones observed in SEM-EDX.

Next, the synthesized **KCFZA** catalysts are used for the hydrogenation of CO_2 to form alcohols in pressurized batch Parr reactors. The catalytic performance of the catalysts was evaluated based on the liquid products formed per unit weight of the catalyst and percentage selectivity of the oxygenates. The gas chromatography (GC) results are shown in Table 1 below.

The **KCFZA** catalysts were able to successfully convert CO_2 to MeOH, but by differing amounts. Trace amounts of other products were also formed in the reaction, including isopropanol (IPA), acetone, and acetic acid (AcOH). *N*-Propanol was detected in such minute amounts that it was almost trivial for comparison. Between **SS1** and **SS1-K**, it was evident that doping the catalyst with *K* increased the selectivity towards EtOH (from 2.5% to 16.3%), which was desirable and corroborates with reported literature data.[7–9] However, there was a significantly stark decrease in ethanol selectivity for **BM1** (1.4%), with almost similar selectivity towards MeOH (95.2%) as **SS1** (96.0%). Conversely, for **BM2** and **BM3**, there was a drastic shift in the selectivity towards AcOH instead of MeOH and EtOH. Specifically, for **BM2** and **BM3**, the MeOH selectivity was 79.6% and 71.8%, respectively, and the AcOH selectivity was 19.1% and 26.6%, respectively. Comparing between **SS1-K**, **BM1** and **BM2**, these three methods used the same metal nitrate salt precursor, albeit different synthesis and preparation methods, yet afforded products with varying selectivities. Most notably, **BM3** produced the most AcOH, *ca.* 40.0 mg $g_{catalyst}^{-1}$ amongst the three mechanochemically-based approaches. Although **SS1-K** and **BM1** are of the same composition, the crystallite size for **BM1** was evidently larger than **SS1-K**, possibly because sintering had occurred due to the heat produced during ball milling. The increase in crystallite size directly decreased the number of active sites, resulting in a decrease in both activity and selectivity towards C_{2+} products. In fact, **BM1** had a product distribution similar to **SS1**, with 95.2% selectivity towards MeOH but a 20% decrease in total yield. **BM2** and **BM3**, on the other hand, demonstrated increased selectivity towards AcOH instead of EtOH. In addition to the difference in crystallite size, TEM-EDX also revealed that mechanosynthesized catalysts had non-homogeneous distribution of the elements, showing phase segregation of Cu, Fe, and Zn. The lower AcOH selectivity on **BM2** was also contributed by the ~10% lower Fe content (4.5% *vs.* 5.0% in **BM3**). This is somewhat similar to a recent report by Tanksale and co-workers who demonstrated the intended formation of AcOH under lower temperature CO_2 reduction, using a framework-based catalyst impregnated with Fe particles and a group I dopant.[28] The observed aggregated zones of increased Cu and Zn content in some of the particles, as observed by SEM and TEM, could have also contributed to the difference in selectivity of the oxygenate products.

From a green chemistry perspective, we endeavoured to also examine and compare the energy consumption and *E*-factor of the synthesis methodologies.[14,29] As the calcination and reduction

Table 1 Relative amounts and selectivity (in parentheses) of products formed based on gas chromatography analysis

	GC analysis mg $g_{catalyst}^{-1}$ (% selectivity)					
S/N	MeOH	EtOH	IPA	Acetone	AcOH	Total
SS1	177.8 (96.0)	4.7 (2.5)	0.2 (0.1)	0.3 (0.1)	2.5 (1.3)	185.5 (100)
SS1-K	138.6 (82.2)	27.7 (16.4)	0.2 (0.1)	0.1 (0.1)	2.0 (1.2)	168.6 (100)
BM1*	141.4 (95.2)	2.1 (1.4)	0.2 (0.2)	0.4 (0.3)	4.3 (2.9)	148.4 (100)
BM2*	123.5 (79.6)	1.4 (0.9)	0.6 (0.4)	0.0 (0.0)	29.6 (19.1)	155.1 (100)
BM3*	107.6 (71.8)	2.0 (1.3)	0.3 (0.2)	0.1 (0.1)	40.0 (26.6)	150.0 (100)

Reaction conditions: catalyst = 100 mg, 15 bar CO_2, 45 bar H_2, 10 mL water, 200 °C, 16 h, * average of 2 runs, % selectivity of the liquid products normalised in ().

steps were used in both solution and solid-state approaches, their energy consumption was also calculated (Supplementary information 18, ESI†). Our calculations revealed that the synthesis methods, which involved the use of solvents, *i.e.* **SS1-K**, consumed the highest total energy per gram of catalyst (4162.6 J g^{-1}) and produced the most amount of liquid waste (1725 mL), hence constituting the highest *E*-factor[29] of 575. Although **BM2** produced less liquid waste (500 mL) and had a lower *E*-factor of 167 than **SS1-K**, it was still mired by the co-precipitation reaction that required a rinsing and drying step during workup, which contributed to its high energy consumption (3979.5 J g^{-1}). **BM3** was the greenest, with the lowest *E*-factor of 0.33 (up to four orders of magnitude in waste reduction) and consumed the least total energy of 2789 J g^{-1} to make the catalyst, utilizing 213 J g^{-1} when only considering the mechanosynthesis and doping step (without calcination and reduction). This corresponds to 86% energy reduction when compared to **SS1-K** (1586.3 J g^{-1}).

Lastly, we conducted a fixed-bed flow reaction using the **KCFZA** catalysts made *via* **BM3**. The reaction was conducted at 200 °C and 50 bar, with a space velocity of 2500 ml(gh)$^{-1}$ using a premixed gas of 4% Ar, 24% CO_2, and 72% H_2 (CO_2 : H_2 in a 1 : 3 ratio). GC analysis (Supplementary information 19, ESI†) revealed that the reactions produced various oxygenates, with comparable selectivity observed for MeOH (30.9%) and EtOH (26.1%), as well as AcOH (35.0%). The formation of AcOH was also observed in the Parr reactor (26.6%), albeit at a slightly lower selectivity. However, the results were significantly different for EtOH, which only marginally formed at 2.0% selectivity in the Parr reactor yet achieved 26.1% selectivity in the flow reactor. Water used as the solvent in the batch reactor could have impeded the formation of EtOH, possibly due to Le Chatelier's principle suppressing the formation of carbon monoxide *via* reverse-water-gas-shift reaction, a key intermediate for EtOH formation.[30]

In conclusion, our experimental results suggest a correlation between the mechanochemically-based methods to synthesise the **KCFZA** catalysts and the selectivity of the products formed. The reaction product became less selective for alcohols and more selective towards AcOH (**BM3** > **BM2** > **BM1** > **SS1-K**), when the catalysts are prepared by more ball milling methods. Whilst the catalyst synthesized *via* **BM3** is the greenest and had the smallest particles, it had the highest selectivity towards AcOH, both in the Parr and flow reactors. This is possibly due to the increased Fe content, caused by friction from the milling auxiliary, which had been shown to promote AcOH formation during CO_2 hydrogenation reactions.[28] Increased Fe could also affect the Brønsted acidity of the catalyst as observed in Cu/Si–Al zeolitic catalysts,[6] but the mechanistic underpinnings are beyond the scope of this work. Even so, it is important to carefully consider the methodologies employed to prepare the catalysts, as they can affect the catalytic outcomes of the reaction. The analyses provided can be tangible examples for researchers in the field of catalysis to explore greener and more sustainable synthesis methodologies.

We acknowledge the support by the Low Carbon Energy Research grant LCERFI01-0033, A*STAR CSF Fund C230415018 and HTCO Seed Fund C231218002. We also thank the Advanced Characterisation and Instrumentation division and Wei En Yeo for their assistance.

Data availability

Additional supporting data have been included as part of the ESI.†

Conflicts of interest

There are no conflicts to declare.

Notes and references

1 S. Solomon, G.-K. Plattner, R. Knutti and P. Friedlingstein, *Proc. Natl. Acad. Sci. U. S. A.*, 2009, **106**, 1704–1709.
2 A. M. Hengne, K. D. Bhatte, S. Ould-Chikh, Y. Saih, J. M. Basset and K.-W. Huang, *ChemCatChem*, 2018, **10**, 1360–1369.
3 M. Aresta and A. Dibenedetto, *Front. Energy Res.*, 2020, **16**, 159.
4 P. Gabrielli, M. Gazzani and M. Mazzotti, *Ind. Eng. Chem. Res.*, 2020, **59**, 7033–7045.
5 D. Xu, Y. Wang, M. Ding, X. Hong, G. Liu and S. C. E. Tsang, *Chem*, 2021, **7**, 849–881.
6 B. Ellis, M. J. Howard, R. W. Joyner, K. N. Reddy, M. B. Padley and W. J. Smith, *Studies Surf. Sci. Catal.*, 1996, **101**, 771–779.
7 E. Heracleous, E. T. Liakakou, A. A. Lappas and A. A. Lemonidou, *Appl. Catal., A*, 2013, **455**, 145–154.
8 B. Xie, R. J. Wong, T. H. Tan, M. Higham, E. K. Gibson, D. Decarolis, J. Callison, K.-F. Aguey-Zinsou, M. Bowker, C. R. A. Catlow, J. Scott and R. Amal, *Nat. Commun.*, 2020, **11**, 1615.
9 D. L. S. Nieskens, D. Ferrari, Y. Liu and R. Kolonko, *Catal. Commun.*, 2011, **14**, 111–113.
10 Y. Chen, S. Choi and L. T. Thompson, *J. Catal.*, 2016, **343**, 147–156.
11 Z. He, Q. Qian, J. Ma, Q. Meng, H. Zhou, J. Song, Z. Liu and B. Han, *Angew. Chem., Int. Ed.*, 2016, **55**, 737–741.
12 H. Kusama, K. Okabe, K. Sayama and H. Arakawa, *Energy*, 1997, **22**, 343–348.
13 K. J. Ardilla-Fierro and J. G. Hernández, *ChemSusChem*, 2021, **14**, 2145–2162.
14 V. K. Singh, A. Chamberlain-Clay, H. C. Ong, F. León, G. Hum, M. Y. Par, P. Daley-Dee and F. García, *ACS Sustainable Chem. Eng.*, 2021, **9**, 1152–1160.
15 R. Tang, H. Wang, S. Zhang, L. Zhang and F. Dong, *J. Colloid Interface Sci.*, 2022, **630**, 290–300.
16 R. Tang, J. Sheng, S. Xi, L. Zhang and F. Dong, *Appl. Catal., B*, 2022, **316**, 121661.
17 L. Yang, Z. Pan, D. Wang, S. Wang, X. Wang, H. Ma, W. Qu and Z. Tian, *Catal. Sci. Tech.*, 2023, **13**, 3796–3803.
18 M. Meng, Y. Shu, Q. Niu and P. Zhang, *Greenhouse Gases: Sci. Technol.*, 2021, **11**, 1198–1212.
19 J. Bao, H. Chen, S. Yang and P. Zhang, *Chin. J. Catal.*, 2020, **41**, 1846–1854.
20 S. H. Hick, C. Griebel, D. T. Restrepo, J. H. Truitt, E. J. Buker, C. Bylda and R. G. Blair, *Green Chem.*, 2010, **12**, 468–474.
21 D. Tan and F. García, *Chem. Soc. Rev.*, 2019, **48**, 2274–2292.
22 K. Ralphs, G. Collins, H. Manyar, S. L. James and C. Hardacre, *ACS Sustainable Chem. Eng.*, 2022, **10**, 6934–6941.
23 Z. Kesic, I. Lukic, M. Zdujic, H. Liu and D. Skala, *Procedia Eng.*, 2012, **42**, 1169–1178.
24 D. Andreeva, I. Ivanov, L. Ilieva, J. W. Sobczak, G. Avdeev and K. Petrov, *Top. Catal.*, 2007, **44**, 173–182.
25 A. Dodd, A. McKinley, T. Tsuzuki and M. Saunders, *J. Eur. Ceram.*, 2008, **29**, 139–144.
26 K. Ralphs, C. Hardacre and S. L. James, *Chem. Soc. Rev.*, 2013, **42**, 7701–7718.
27 D. Xu, M. Ding, X. Hong and G. Liu, *ACS Catal.*, 2020, **10**, 14516–14526.
28 W. Ahmad, P. Koley, S. Dwivedi, R. Lakshman, Y. K. Shin, A. C. T. van Duin, A. Shrotri and A. Tanksale, *Nat. Commun.*, 2023, **14**, 2821, DOI: 10.1038/s41467-023-38506-5.
29 R. A. Sheldon, *Green Chem.*, 2007, **9**, 1273–1283.
30 S. S. Ali, S. S. Ali and N. Tabassum, *J. Environ. Chem. Eng.*, 2022, **10**, 106962.